JOURNAL OF THERMOPHYSICS AND HEAT TRANSFER
Vol. 22, No. 4, October–December 2008

Heat Transfer Investigation in Evaporator of Loop Heat Pipe During Startup

M. A. Chernysheva* and Y. F. Maydanik†
Institute of Thermal Physics, 620016, Ekaterinburg, Russia
and
J. M. Ochterbeck‡
Clemson University, Clemson, South Carolina 29634

DOI: 10.2514/1.35519

The problem of startup heating for a cylindrical evaporator of a loop heat pipe when the evaporator is completely filled initially with liquid has been examined. A two-dimensional mathematical heat transfer model has been formulated for this problem, for which the system of differential heat conduction equations was solved numerically. Modeling of the heat transfer processes in a cylindrical evaporator was conducted for different thermal regimes. The effects of the evaporator geometrical parameters and the thermophysical properties of materials during the formation of the temperature field were investigated. The results are presented in the analysis of the main factors that influence the dynamics of the evaporator startup.

Nomenclature

a	=	thermal diffusivity, $m^2 \cdot s^{-1}$
c	=	specific heat, $J \cdot kg^{-1} \cdot K^{-1}$
E_1	=	copper–copper (Cu–Cu) evaporator
E_2	=	stainless-steel–nickel (SS–Ni) evaporator
g	=	gravitational acceleration, $m \cdot s^{-2}$
h	=	thickness of liquid layer, m
Q	=	heat load, W
q	=	heat flux, $W \cdot m^{-2}$
L_q	=	length of heat-supply zone, m
r	=	coordinate in radial direction
d	=	diameter, m
S_q	=	area of applied heat load, m^2
T	=	temperature, °C
τ	=	time, s
z	=	coordinate in the z direction
β	=	coefficient of volumetric expansion, K^{-1}
δ	=	thickness, m
ε	=	porosity
λ	=	thermal conductivity, $W \cdot m^{-1} \cdot K^{-1}$
μ	=	dynamic viscosity, $Pa \cdot s$
ν	=	kinematic viscosity, $m^2 \cdot s^{-1}$
ρ	=	density, $kg \cdot m^{-3}$

Subscripts

av	=	average
cc	=	central core
eb	=	evaporator body or wall
ev	=	evaporator
l	=	liquid
max	=	maximum
min	=	minimum
p	=	parasitic
w	=	wick
0	=	initial

Received 7 November 2007; accepted for publication 18 February 2008.

*106 Amundsen Street; maidanik@etel.ru.
†106 Amundsen Street.
‡Department of Mechanical Engineering; jochter@clemson.edu.

I. Introduction

LOOP heat pipes (LHPs) are highly efficient heat transfer devices operating on a closed evaporation–condensation cycle. They are capable of functioning at any orientation with respect to gravity and transferring heat over sufficiently large distances. The circulation of the working fluid in an LHP is driven by the capillary pressure created by the liquid–vapor menisci in the capillary wick structure. The schematic diagram of the device is given in Fig. 1. The main elements of an LHP are an evaporator, a condenser, a vapor line, and a liquid line. The heat load transported by the LHP is supplied to the evaporator and removed from the condenser.

LHPs have many applications in different fields of engineering. They are used successfully in thermoregulation systems of spacecraft, for cooling components of electronic devices and computer equipment, for low-grade-heat recovery, and for several other purposes connected with heat transfer [1–4].

The LHP theory is regarded as sufficiently well developed for stationary operating regimes [5,6]. The methods of design calculation of the main elements of the LHP have been suggested on the basis of this theory, and practical recommendations with respect to the choice of a working fluid and the optimal dimensions of the capillary structure have been determined. Numerous papers on this subject, and also papers devoted to experimental and analytical investigations of LHPs, have been published [7–9]. Good agreement between the results of the calculations and the experimental data makes it possible to provide a good description of the physical processes observed in LHPs.

Currently, one of the most urgent problems requiring the investigation and development of two-phase loops with capillary pumping remains the provision of a reliable startup. This problem is specific to the LHP and is connected with the design features and physical principles of operation of these devices. It manifests itself in the fact that relatively small heat loads supplied to the evaporator do not result in the formation of the necessary temperature difference required for providing the circulation of a working fluid and a stationary temperature level. Instead, one can observe a continuous rise of temperature in the heat-supply zone of the evaporator. As a result, the available range of LHP heat loads proves to be limited not only by a maximum, but also by a minimum. Therefore, it is necessary to examine the minimum heat load for an LHP startup.

The investigations devoted to this problem mainly contain analysis and generalization of experimental data. For example, considerable variations exist in the experimental data on minimum startup loads and also the overall LHP behavior during startup, which are indicative of sensitivity to the LHP parameters and the effect of

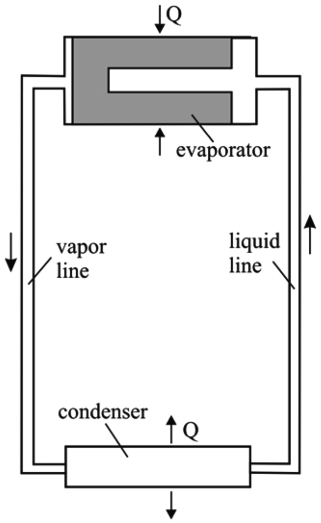

Fig. 1 Scheme of the loop heat pipe.

the environment [10]. A previous investigation [11] studied the effect of the gravitation field, the temperature in the condenser, and the heat load supplied on the time it takes for for an LHP to reach a stationary serviceable state. When researching startup regimes of a miniature LHP with a disk-shaped evaporator, Singh et al. found that the startup time for a low heat load is more than that for a high heat load [12]. A previous study [13] established that the prestart state in the LHP evaporator determines to a great extent the device behavior during startup. On the bases of the analysis of the experimental data, the LHP startup regimes have been classified. According to this classification, there are four typical LHP scenarios during startup (Fig. 2). The main determining factors of the behavior are the degree of liquid fill in the evaporator and the position of the liquid–vapor interfaces. The first and second scenarios of the startup are characterized by the fact that the vapor removal channels are filled with the liquid and, in startup diagrams, one can see a sharp peak, which fixes the moment of liquid boiling up in the vapor removal channels and the beginning of working liquid circulation. In Rodriquez et al. [14], the results of the experimental startup research for a propylene LHP are presented. The authors point to the fact that the startup result of an LHP with vapor removal channels filled with liquid can be excessive temperature overshoots. To address that problem, they proposed using an auxiliary startup heater placed either on the transition tube or on the evaporator flange. Kaya et al. developed a numerical model to simulate the startup performance characteristics of an LHP for the second prestart situation, during which the vapor removal channels are filled with liquid and the compensation chamber is two phase [15]. A global loop model has been designed by using a lumped parameter code (SINDA/FLUINT) for the simulation of startup conditions in a propylene LHP [16]. This model is based on the assumption that the vapor phase is present both in the vapor removal channels and in the compensation chamber; thus, the third and the fourth startup scenarios were researched.

The prestart situation 1 in the evaporator shown in Fig. 2 has been chosen for this investigation. It corresponds to an LHP startup with an orientation of $\varphi = -90$ deg when the condenser is above the evaporator. A similar situation also may be observed in conditions with reduced gravitation.

It is well known that the startup of an LHP from a fully flooded state includes two main stages:

1) The heating of the evaporator after the supply of a heat load. At this stage, a nonstationary temperature field forms.

2) The boiling of the working fluid followed by transition to a stationary operating regime.

An analysis of experimental data shows that the first stage of startup is determined only by the evaporator parameters and the second by the parameters of the entire heat transfer device. In the first stage of investigation, it was decided to restrict the consideration only to the first stage to determine the degree of influence of the

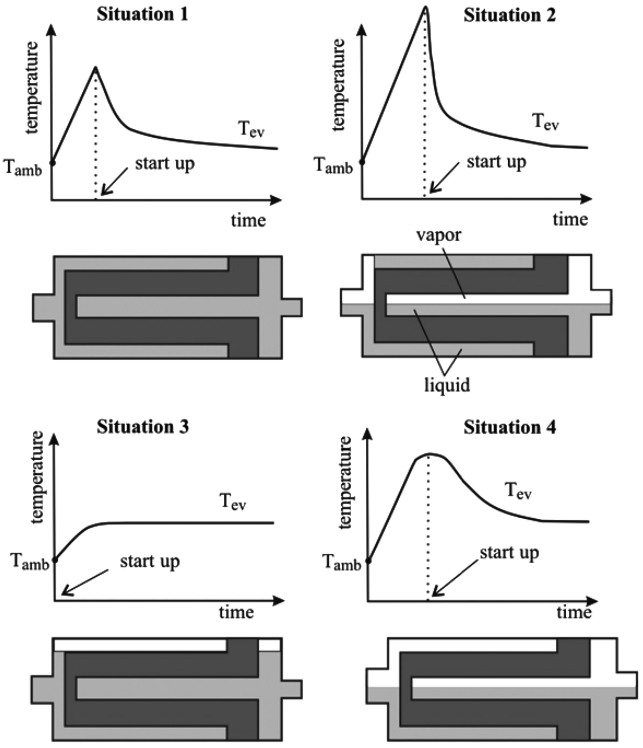

Fig. 2 Possible prestart situations and their influence on the LHP startup.

evaporator parameters on the heating dynamics, which directly affects the LHP startup behavior and characteristics.

The aim of the present investigation is to study the characteristics of the first stage of an LHP startup when the evaporator is in a fully flooded state. The main task of the investigation is to model numerically the heating of an LHP cylindrical evaporator and reveal the main factors that influence the formation of the temperature field in the evaporator.

II. Physical Model

This investigation examines the problem of temperature field formation in a cylindrical LHP evaporator completely filled with liquid (Fig. 2). A more detailed scheme of the evaporator and the heat-supply zone with a heat load Q is shown in Fig. 3a. The heat flux density q is constant in regards to the heated area S_q:

$$q = \frac{Q}{S_q} \tag{1}$$

where $S_q = 2 \cdot \pi \cdot r_3 \cdot L_q$, r_3 is the evaporator radius, and L_q is the length of the heated zone (active zone).

The evaporator is an object with a complicated geometry (Fig. 3a) whose main elements are the evaporator body, the wick, the compensation chamber, and central core. The thermophysical characteristics of the evaporator materials, such as the heat capacity c_p, thermal conductivity λ, and density ρ, are designated by corresponding indices i ($i = 1$, evaporator body; $i = 2$, wick; $i = 3$, liquid). The length of the heated zone L_q is equal to the distance Z_1Z_3. For the model under discussion, the following criteria and assumptions have been adopted:

1) Convective processes do not play a role in heat transfer. Heat transfer is realized by conduction. In the general case, it is rather a rough assumption as the object under study contains a fluid, present both in the central core and in the compensation chamber. Also, the wick is saturated with a liquid. The substantiation of this assumption may be as follows:

First, it is well known that natural convection is hampered in the wick as the liquid in the pores is bounded. Second, for the region of the wick, central core, and compensation chamber, this assumption is

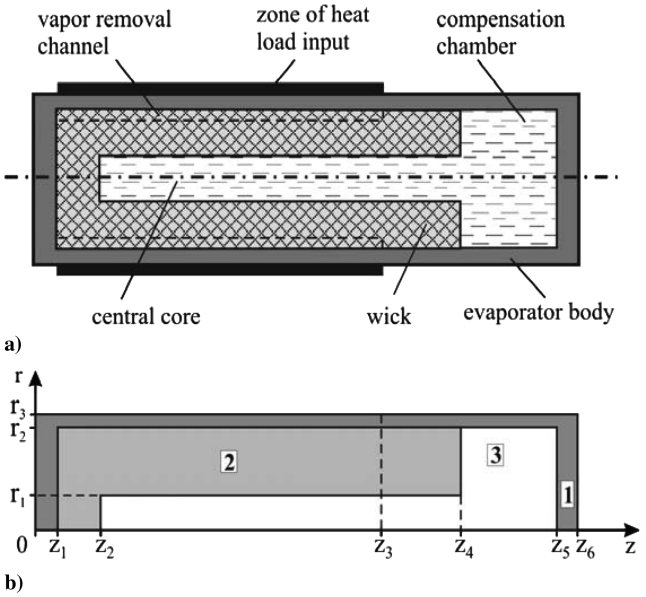

Fig. 3 Scheme of the cylindrical evaporator (a) and the calculation domain (b).

also sufficiently correct in the modelling of thermal processes in the evaporators of miniature LHPs whose outer diameters do not exceed 8 mm. The diameter of the central core of miniature evaporators may range from 0.5 to 2 mm. Natural convection is hampered in such narrow channels. Actually, it is well known that natural convection is practically absent if

$$Gr \cdot Pr < 1000 \tag{2}$$

where $Gr \cdot Pr = g \cdot \beta \cdot h^3 \times \rho_l \cdot \Delta T / \mu \cdot \alpha$ is the product of the Grashof number and the Prandtl number, which characterizes the intensity of heat exchange by natural convection. From this relation, one can find the limiting thickness of the liquid layer where convection is insignificant. Thus, for water in the temperature range of 20–100°C and for temperature gradients, ΔT, of 2–10°C, the limiting thickness of the layer and, consequently, the channel size is from 1.2 to 2.4 mm.

As for the compensation chamber, its dimensions are also sufficiently small. Besides, it is typically assumed that in the compensation chamber there is a secondary wick, which prevents the origination of natural convective processes. The model under discussion also may be used for evaporators with larger diameters if a secondary wick is found in both the compensation chamber and central core.

2) The evaporator is thermally insulated everywhere with the exception of the heat-supply zone. Thus, the heat exchange with the environment at the outer surface is not taken into account.

3) Ideal thermal contact exists between the evaporator body and the wick, which may be achieved, for instance, by soldering the wick to the body.

4) The heat transfer coefficient between the wick and the liquid is high. Therefore, the liquid and solid phases are in local thermodynamic equilibrium. Consequently, the temperatures in every small elementary volume are the same.

5) The effective thermal conductivity, the heat capacity, and the density of the wick are determined as follows:

$$\lambda_2 = \lambda_l \cdot \varepsilon + \lambda_w \cdot (1 - \varepsilon) \tag{3}$$

$$c_2 \cdot \rho_2 = c_l \cdot \rho_l \cdot \varepsilon + c_w \cdot \rho_w \cdot (1 - \varepsilon) \tag{4}$$

III. Mathematical Formulation of the Problem

The problem was solved using a two-dimensional transient formulation in cylindrical coordinates r and z. Given the problem symmetry with respect to the central axis of the cylinder, a half-domain section was used in the calculation (Fig. 3b). The mathematical model includes the heat transfer equations for each of the three design elements forming the evaporator as a single object:

$$\frac{\partial T}{\partial \tau} = a_i \cdot \left(\frac{\partial^2 T}{\partial r^2} + \frac{1}{r}\frac{\partial T}{\partial r} + \frac{\partial^2 T}{\partial z^2} \right) \tag{5}$$

where

$$a_i = \lambda_i / (c_i \cdot \rho_i) \tag{6}$$

Initial conditions:

$$\tau = 0, \qquad T(r, z) = T_0 \tag{7}$$

Boundary conditions:

1) Outer wall of the evaporator in the heat-supply zone:

$$z_1 < z < z_3, \qquad r = r_3 : \qquad \lambda_1 \frac{\partial T}{\partial r} = -q \tag{8}$$

2) Outer wall of the evaporator, with the exception of the heated zone:

$$\begin{aligned} &z_3 < z < z_6 \quad \text{and} \quad 0 < z < z_1, \qquad r = r_3 : \qquad \frac{\partial T}{\partial r} = 0 \\ &0 < r < r_3 \quad \text{and} \quad z = 0, \qquad z = z_6 : \qquad \frac{\partial T}{\partial z} = 0 \end{aligned} \tag{9}$$

3) Internal boundaries at contact sites:

$$\lambda^* \frac{\partial T}{\partial n}\bigg|_c = \lambda^{**} \frac{\partial T}{\partial n}\bigg|_c \tag{10}$$

where C is the coordinate of a boundary surface, n is the normal at a point C, and λ^* and λ^{**} are the thermal conductivity coefficients of corresponding maters.

4) Symmetry axis of the cylinder:

$$0 < z < z_6, \qquad r = 0 : \qquad \frac{\partial T}{\partial r} = 0 \tag{11}$$

IV. Solution Procedure

The system of partial differential equations was solved numerically. The energy balance method was chosen for obtaining a numerical formulation for the problem of heat transfer in a cylindrical evaporator. An explicit scheme of the solution was applied. In the numerical realization of the solution, a uniform grid for the time coordinate and a piece uniform for the spatial coordinates were used given the odd-shaped regions of the evaporator, which were divided into subregions. The size of the spatial step for every subregion was chosen with allowance for two conditions: efficiency in the calculation time and sufficient number of nodes in every calculated subregion. The total number of grid nodes was 22 in the r axis direction and 62 in the z axis direction . Thus, meshes of 22×62 were tested. The time step $\Delta\tau$ was chosen from the condition of provision of stability for the difference scheme, that is,

$$\Delta\tau \le \min(\Delta\tau_j)$$

where

$$\Delta\tau_j = (\Delta h_j)^2 / (4 \cdot \alpha_j) \qquad \Delta h_j \le \min(\Delta r_j, \Delta z_j)$$

where α_j is the thermal diffusivity of a material, and Δr_j and Δz_j are spatial steps in the j subregion.

V. Results

The results of the calculations yielded temperature fields in the evaporator, which make it possible to follow the heating process and analyze the main characteristics of conduction heat transfer in the

body of a complicated LHP evaporator geometry. The results presented here are for miniature evaporators, with diameters equal to 6 or 6.5 mm and a total evaporator length of 40 mm. The heating-zone length was 20 mm. "Traditionally" used combinations of materials, such as copper–copper (evaporator E_1) and stainless-steel–nickel (evaporator E_2) were used as materials for the evaporator body and the wick. Investigations were made with water as the working fluid and a 60% porosity of the wick.

Figure 4 gives an example of the isotherm fields for an evaporator, to which a heat load of 5 W was supplied. The evaporator initial temperature was 22°C, the evaporator body is stainless steel, and the wick is nickel (E_2). From these diagrams, one can follow the evolution of the evaporator heating process. It is seen that 1 s after the application of the heat load (Fig. 4a) the temperature has changed only in a small region close to the heating zone, whereas the rest of the evaporator is still cold. Five seconds after (see Fig. 4b) applying heat to the active region, the temperature field increased. The temperature reaches its highest values in the heated section and decreases monotonically from it in both the axial and radial directions. In Fig. 4c, one can see how far from the heating zone the temperature front moved in the compensation chamber direction in the time interval $\Delta\tau = 10$ s after applying heat. It should be mentioned that a significant part of the heat propagation is provided along the evaporator body. The last diagram in Fig. 4d illustrates the situation in the evaporator within 15 s of initiating heating. In the vicinity of the heated wall, the temperature increased considerably. The difference between the average temperature T_{av} in the heated zone and the initial temperature T_0 is $T_{\text{av}} - T_0 = 36$°C, and the difference between the temperature values at the highest $T_{\max}$ and lowest $T_{\min}$ is $T_{\max} - T_{\min} = 38$°C.

A. Formation of Wick Wall Temperature Difference

One of the most significant parameters characterizing the startup situation in the evaporator is the value of the temperature difference between the outer and the inner surface of the wick ΔT_w. Owing to the specific character of the evaporator geometry and the location of the heat-supply zone one, can observe considerable nonuniformity in the temperature distribution both at the inner surface of the wick and in the heating zone (Fig. 4). Therefore, for analysis, it is more convenient to use the following two values of $\Delta T_{\max}$ and ΔT_{av} to characterize the temperature differences on the wick:

$$\Delta T_{\max} = T^{\text{ex}}_{\max} - T^{\text{in}}_{\max} \tag{12}$$

where $T^{\text{in}}_{\max}$ is the maximum temperature at the inner surface of the wick S_{in}, and $T^{\text{ex}}_{\max}$ is the maximum temperature in the applied heat zone S_q. All other factors being equal, the boiling initiation of the working fluid will most likely take place at the most heated point, that is, where the temperature is a maximum. Therefore, it is necessary to trace such "weak" spots and also temperature values as they characterize the degree of local superheat of the liquid:

$$\Delta T_{\text{av}} = T^{\text{ex}}_{\text{av}} - T^{\text{in}}_{\text{av}} \tag{13}$$

where $T^{\text{in}}_{\text{av}}$ is the average temperature at the inner surface of the wick S_{in}, and $T^{\text{ex}}_{\text{av}}$ is the average temperature in the applied heat zone. Average temperatures are calculated by

$$T_{\text{av}} = \frac{1}{S}\int T(s)\,\mathrm{d}s \tag{14}$$

where $T(s)$ is the temperature distribution over the surface S, and T_{av} is the average temperature over the surface S.

Figures 5 and 6 present the differences $\Delta T_{\text{av}}(\tau)$ and $\Delta T_{\max}(\tau)$ for two similar evaporators, which differ only in the thickness of the wick wall δ_w. The thickness δ_w varied with changes in the diameter of the central core d_{cc}. In the first evaporator $d_{\text{cc}} = 1$ mm, whereas in the other evaporator $d_{\text{cc}} = 2$ mm. As may be seen from the plots (Figs. 5 and 6), certain effects are traced in the heating of the evaporators at different heat loads Q. The initial stage of heating is characterized by a high rate of increase of $\Delta T_{\max}$. Later, the rate of increase of $\Delta T_{\max}$ decreases and then, on achieving a maximum value, practically does not change with time. The gently sloping section of the curve corresponds to the later part in the plot. It means that, though one can observe here constant heating with respect to time of the evaporator in its entirety (Figs. 4 and 6), the primary difference in $\Delta T_{\max}$ forms only at the initial stage (Fig. 5).

B. Parasitic Heat Flow

The analysis of the experimental results has shown that the main reason for difficulties in LHP startup, especially at low heat loads, is a considerable amount of parasitic heat flow from the heating zone into the compensation chamber and the central core of the wick. For miniature LHPs this problem is particularly pressing, due to the fact that the evaporator dimensions are small. The possibility of spatially

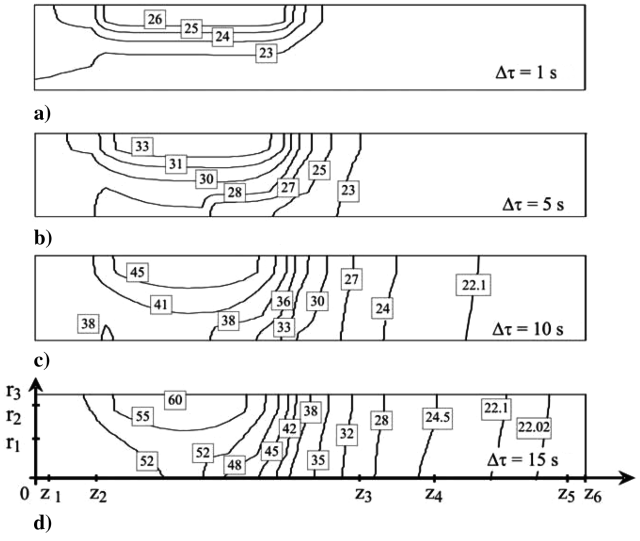

Fig. 4 Temperature evolution of the LHP cylindrical evaporator (E_2). $Q = 5$ W.

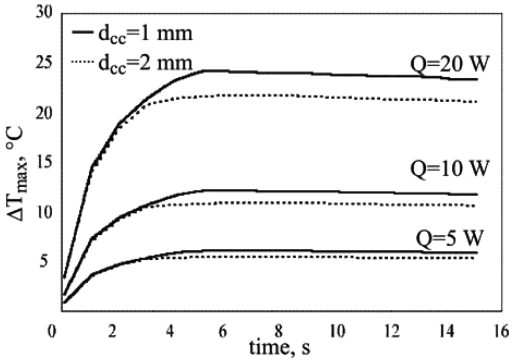

Fig. 5 Formation of $\Delta T_{\max}$ during startup for E_2.

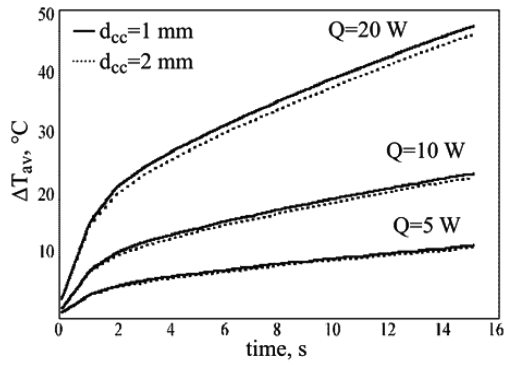

Fig. 6 Formation of ΔT_{av} during startup for E_2.

separating the heating zone and the inner absorbing surface of the wick formed by the central core is quite limited. The relatively small thickness of the wick also makes its inner surface a potential place for liquid boiling. According to the main principles of LHP operation, this is very undesirable and means, in fact, a startup failure as for the evaporator variant under discussion intensive evaporation is needed to take place close to the heated wall in the evaporation zone. A decrease in the heating of the evaporator interior may be achieved by decreasing parasitic heat flows. Knowing the temperature distributions in the evaporator, the parasitic heat that penetrates into the central core and the compensation chamber can be evaluated. Because heat is propagated both through the wick Q_w and over the body of the evaporator Q_{eb}, it is possible to take into account the contribution of each and analyze the main contributing factors.

C. Effect of Evaporator Internal Characteristics on Temperature Field Formation

1. Effect of Thermal Conductivity of Wick and Evaporator Body

The thermal conductivities of the wick and the evaporator body are main factors that influence the temperature field formation in the evaporator. Figures 7 and 8 present the results of calculating $Q_p^*(t)$ and $\Delta T_{\max}(\tau)$ for two similar evaporators. Here, Q_p^* is the relative value of parasitic flows determined as

$$Q_p^* = (Q_p/Q) \cdot 100\% \tag{15}$$

The geometrical characteristics of the evaporators examined were the same. One of the evaporators, E_1, had a copper body ($\lambda_1 = 390$ W/m · K) and a copper wick ($\lambda_2 = 40$ W/m · K), wheras the second, E_2, had a stainless-steel body ($\lambda_1 = 17$ W/m · K) and a nickel wick ($\lambda_2 = 3$ W/m · K). The heat load supplied was 5 W. The plots show how strongly the thermal conductivity of the materials affects the values of the parasitic heat flow and also the temperature distribution in the evaporator. The use of high thermal conductivity materials for the evaporator leads to a more uniform heating of the entire evaporator. When materials with a low thermal conductivity are used in the evaporator, a larger temperature gradient zone near the heated wall develops. The increased rate of local heating ensures, first, local liquid boiling and, second, that a shorter prestart period of boiling is expected, determined from the moment of applying the external heat load until the formation of a vapor phase in this zone. Based on this effect, it is possible to make the following recommendation for the material selection of the evaporator body and the wick: preference should be given to materials with a relatively low thermal conductivity.

2. Effect of Thickness of Wick Wall

From Figs. 5 and 6, the wick wall thickness effects are seen in the difference of temperatures $\Delta T_{\text{av}}(\tau)$ and $\Delta T_{\max}(\tau)$. The higher the heat load supplied, the more noticeable the effect. Figure 9 gives plots of the dependence $Q_p^*(\tau)$ for two values of δ_{wick}. Quite significant is the following fact: an increase in the wick wall thickness of only 0.5 mm leads to a considerable (up to 3 times) decrease of Q_p^*. Thus, quite justified are the aspirations to spatially separate the outer and the inner surface of the wick by increasing the wick thickness, though this is not always justified from the viewpoint of hydraulic losses in the wick. Nevertheless, the increase of δ_w may be regarded as one of the possible means to avoid liquid superheats in the central core and, consequently, liquid boiling. Because heat flows both over the evaporator body Q_{eb} and through the wick Q_w, both make contributions to the value of Q_p:

$$Q_p = Q_w + Q_{\text{eb}} \tag{16}$$

The contribution of each component shall be examined.

Figures 10 and 11 present the results $Q_p(\tau)$, $Q_w(\tau)$, and $Q_{\text{eb}}(\tau)$ over a 15 s startup time interval. One can see that for an evaporator with a thin-walled wick (Fig. 10) the main contribution to Q_p is made by Q_w. An insignificant increase in the wick wall thickness, δ_{wick}, may result in the change of the relations between Q_w and Q_{eb} (Fig. 11). First, it happens at the expense of decreasing Q_w, whereas the values of heat flow over the body do not practically change. The characteristic shape of the curves $Q_{\text{eb}}(\tau)$ and $Q_w(\tau)$ makes it possible to say that the value of Q_w is actively formed in the initial period of

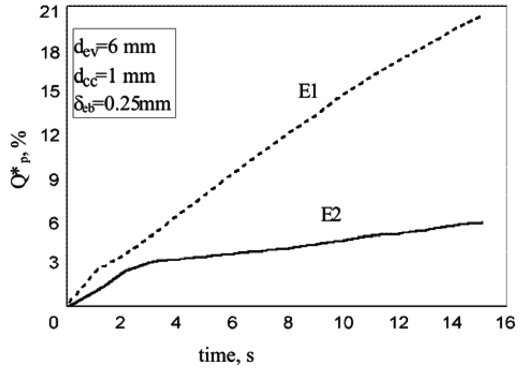

Fig. 7 Effect of λ_1 and λ_2 on Q_p^*. $Q = 5$ W.

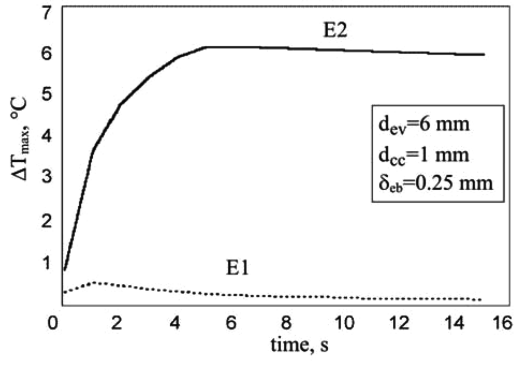

Fig. 8 Effect of λ_1 and λ_2 on $\Delta T_{\max}$. $Q = 5$ W.

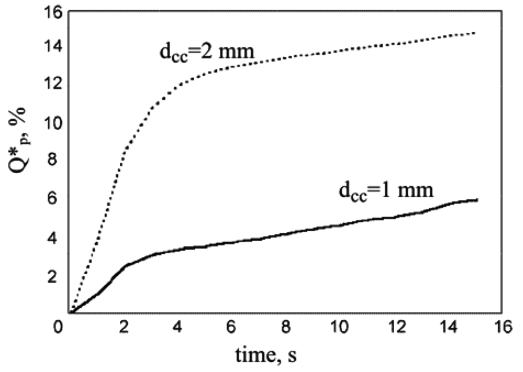

Fig. 9 Effect of the wick wall thickness on Q_p^* for E_2. $Q = 20$ W.

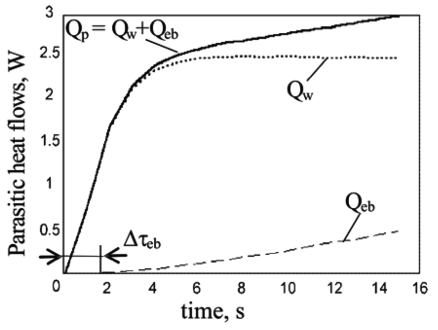

Fig. 10 Relation between Q_p, Q_w, and Q_{eb} for E_2. $Q = 20$ W, $d_{\text{ev}} = 6$ mm, and $d_{\text{cc}} = 2$ mm.

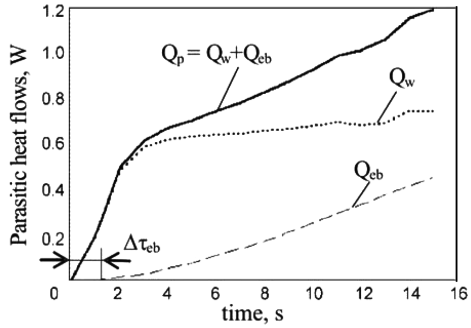

Fig. 11 Relation between Q_p, Q_w, and Q_{eb} for E_2. $Q = 20$ W, $d_{ev} = 6$ mm, and $d_{cc} = 1$ mm.

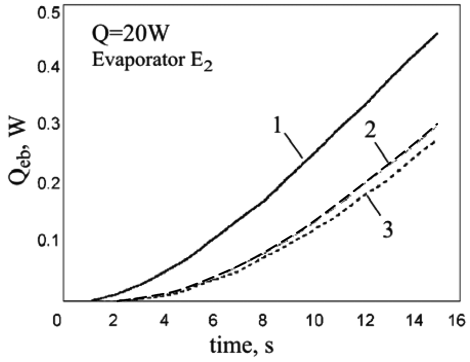

Fig. 12 Effect of the body wall thickness, δ_{eb}, on Q_{eb}: 1) $d_{ev} = 6$ mm, $\delta_{eb} = 0.25$ mm, 2) $d_{ev} = 6$ mm, $\delta_{eb} = 0.5$ mm, and 3) $d_{ev} = 6.5$ mm, $\delta_{eb} = 0.5$ mm.

the evaporator heating. Then, upon reaching a maximum, it remains practically unchanged with further time increases. At the same time, Q_{eb} tends to constantly increase with time. It is possible to single out a certain initial time interval $\Delta\tau_{eb}$ when parasitic flows over the body Q_{eb} are so small that the contribution to Q_p may be neglected. The value of $\Delta\tau_{eb}$ characterizes the speed of the temperature front movement over the evaporator body in the direction of the compensation chamber. Its value depends on the distance the compensation chamber is removed from the heating zone.

3. Effect of Evaporator Body Wall Thickness

As mentioned, part of the heat supplied penetrates into the compensation chamber, which increases the liquid temperature. This circumstance should also be taken into account for avoiding considerable liquid superheats, which may lead to boiling in the compensation chamber before the vapor phase appears and begins to expand in the evaporation zone. Figure 12 presents the results of $Q_{eb}(\tau)$ as a function of the thickness of the evaporator wall, δ_{eb}, for the evaporator E_1. Particularly noteworthy is the fact that, with increasing δ_{eb}, heat flows in the compensation chamber over the body at the initial instant of time decrease. This circumstance is a manifestation of "the effect of an attached mass," due to the fact that increasing thickness of the evaporator body wall results in an increase in its mass. Thus, more energy is required for increasing the evaporator body temperature. Besides, it is favored by the higher thermal conductivity of the evaporator wall λ_1, which exceeds the thermal conductivity of the liquid λ_3 approximately 30 times. Such a situation produces a positive effect on the startup process even with the use of more heat-conducting materials, such as copper in particular.

VI. Conclusions

A mathematical model is presented for the numerical modelling of transient heat processes in the cylindrical evaporator of a loop heat pipe. The model has been developed for one possible prestart situation in which the evaporator is completely filled with a liquid. The problem took into account the main characteristics of the evaporator geometry. The effects of the evaporator geometrical parameters, the thermophysical properties of the evaporator materials, and the heat load supplied on the temperature distribution were investigated numerically. The primary characteristics in the dynamics of heating have been established. Several recommendations are suggested on the basis of the obtained results, which makes it possible to avoid negative results in LHP startup.

References

[1] Maydanik, Y. F., and Fershtater, Y. G., "Theoretical Basis and Classification of Loop Heat Pipes and Capillary Pumped Loops," *Proceeding of the 10th International Heat Pipe Conference*, 1997.

[2] Bienart, W., and Wolf, D., "Temperature Control with Loop Heat Pipes: Analytical Model and Test Results," *Proceeding of the 9th International Heat Pipe Conference*, Los Alamos National Laboratory, Los Alamos, NM, 1995, pp. 981–987.

[3] Pastukhov, V. G., Maydanik, Y. F., Vershinin, C. V., and Korukov, M. A., "Miniature Loop Heat Pipes for Electronics Cooling," *Applied Thermal Engineering*, Vol. 23, No. 9, June 2003, pp. 1125–1135. doi:10.1016/S1359-4311(03)00046-2

[4] Maydanik, Y. F., "Loop Heat Pipes—Development and Application," *Proceeding of the 7th International Heat Pipe Symposium*, Heat Pipe Section, Korean Society of Mechanical Engineers, Seoul, Korea, 2003, pp. 45–61.

[5] Maydanik, Y. F., Fershtater, Y. G., and Pastukhov, V. G., *Loop Heat Pipes: Development, Research, Elements of Engineering Solution*, Ural Branch of USSR Science Academy, Sverdlovsk, Russia, 1989.

[6] Kaya, T., Hoang, T. T., Ku, J., Cheung, M.K., "Mathematical Modeling of Loop Heat Pipes," AIAA Paper 99-0477, 1999.

[7] Ku, J., "Operating Characteristics of Loop Heat Pipes," Society of Automotive Engineers Paper 1999-01-2007, 1999.

[8] Chernysheva, M. A., Maydanik, Y. F., and Vershinin, S. V., "Heat Exchange in the Evaporator of a Loop Heat Pipe with a Biporous Capillary Structure," *Proceeding of the 11th International Heat Pipe Conference*, Japan Association for Heat Pipes, Kumamoto, Japan, 1999, pp. 69–75.

[9] Solodovnik, N. N., Maydanik, Y. F., and Fershtater, Y. G., "Methods of Loop Heat Pipe Regulation," *Proceeding of the International Workshop "Heat Pipes, Heat Pumps, Refrigerators"*, Luikov Heat and Mass Transfer Institute, Academy of Sciences of Belarus, Minsk, Belarus, 1995.

[10] Yendler, B., Baumann, J., and Cullimore, B., "Summary of Design Parameters of CPL/LHP Components," *Proceeding of the CPL '98 International Workshop "Capillary Pumped Two-Phase Loops,"* Aerospace Corporation, El Segundo, CA, 1998, pp. 1.6-2–1.6-5.

[11] Kiseev, V. M., "Transient and Start-Up Behavior of Loop Heat Pipes Due to Gravity," *Proceeding of the 12th International Heat Pipe Conference*, Institute of Thermal Physics, Ural Branch, Russian Academy of Sciences, Ekaterinburg, Russia, 2002, pp. 114–119.

[12] Singh, R., Akbarzaden, A., and Dixon, C., "Thermal Characteristics of the Miniature Loop Heat Pipe with Water as the Working Fluid," *Proceeding of the 8th International Heat Pipe Symposium*, Japan Association for Heat Pipes, Kumamoto, Japan, 2006, pp. 191–196.

[13] Maydanik, Y. F., Solodovnik, N. N., and Fershtater, Y. G., "Investigation of Dynamic and Stationary Characteristics of a Loop Heat Pipe," *Proceeding of the 9th International Heat Pipe Conference*, Los Alamos National Laboratory, Los Alamos, NM, 1995, pp. 1002–1006.

[14] Rodriquez, J. I., Pauken, M., and Na-Nakornpanom, A., "Transient Characterization of a Propylene Loop Heat Pipe During Startup and Shut-Down," Society of Automotive Engineers, Inc. Paper 2000-01-2408, 2000.

[15] Kaya, T., Pérez, R., Gregori, C., and Torres, A., "Numerical Simulation of Transient Operation of Loop Heat Pipes," *Applied Thermal Engineering*, Vol. 28, Nos. 8–9, June 2008, pp. 967–974.

[16] Zinna, S., Marengo, M., and Cossali, G. E., "Numerical Simulation of a Propylene LHP: Stationary and Start-Up Conditions," *Proceeding of the 14th International Heat Pipe Conference*, Federal University of Santa Catarina, Mechanical Engineering Department, Florianopolis/SC – Brazil, 2007, pp. 342–347.